THE JOURNAL OF PHYSICAL CHEMISTRY Letters

Letter

pubs.acs.org/JPCL

Anomalous Structural Disorder in Supported Pt Nanoparticles

Fernando D. Vila,*[,†] John J. Rehr,[†] Ralph G. Nuzzo,[‡] and Anatoly I. Frenkel[§,∥]

[†]Department of Physics, University of Washington, Seattle, Washington 98195, United States

[‡]Department of Chemistry, University of Illinois, Urbana, Illinois 61801, United States

[§]Department of Materials Science and Chemical Engineering, Stony Brook University, Stony Brook, New York 11794, United States

[∥]Division of Chemistry, Brookhaven National Laboratory, Upton, New York 11973, United States

Supporting Information

ABSTRACT: Supported Pt nanocatalysts generally exhibit anomalous behavior, including negative thermal expansion and large structural disorder. Finite temperature DFT/MD simulations reproduce these properties, showing that they are largely explained by a combination of thermal vibrations and low-frequency disorder. We show here that a full interpretation is more complex and that the DFT/MD mean-square relative displacements (MSRD) can be further separated into vibrational disorder, "dynamic structural disorder" (DSD), and long-time equilibrium fluctuations of the structure dubbed "anomalous structural disorder" (ASD). We find that the vibrational and DSD components behave normally, increasing linearly with temperature while the ASD decreases, reflecting the evolution of mean nanoparticle geometry. As a consequence the usual procedure of fitting the MSRD to normal vibrations plus temperature-independent static disorder results in unphysical bond strengths and Grüneisen parameters.

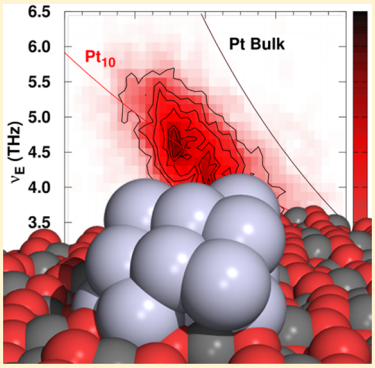

Supported metal nanoparticles (NPs) are widely used as catalysts in applications ranging from chemical synthesis to petroleum refining.[1,2] Consequently, their nanoscale structure and behavior are of considerable technological interest. Their properties as a function of size, temperature, and interaction with the support are important determinants of catalytic activity and selectivity. However, understanding their behavior is challenging due partly to their inhomogeneous structure and substantial differences versus the bulk, especially at high operating temperatures and in the presence of support and ligands.[3−5] EXAFS studies of nanoscale Pt clusters on γ-Al_2O_3 reveal several anomalous properties:[6,7] First, EXAFS analysis[6] shows that ∼1 nm NPs exhibit negative thermal expansion (NTE) and have shorter average Pt−Pt bond lengths than in bulk Pt. In contrast, ∼2.9 nm NPs have positive thermal expansion on average and mean bond lengths closer to those in the bulk. Using DFT/MD simulations,[8,9] this behavior was attributed to "dynamic structural disorder" (DSD), that is, the inhomogeneous, fluctuating nature of structure on the nanoscale. In particular, the DSD exhibits multiple time scales, being driven by the chaotic motion of the center of mass (CM) of the NPs, their librational motion, and transient tethering to the support on the picosecond time scale and their internal fluxional bonding on substantially slower time scales. Second, EXAFS data for small NPs exhibit unusually large Pt−Pt bond length fluctuations, that is, mean-squared relative-displacements (MSRD), compared with vibrational motion at T = 0 K. These quantities are important for interpreting vibrational properties such as bond strengths and Grüneisen parameters. Our main goal here is to understand this behavior. The large corrections to the zero-point MSRD are usually interpreted as temperature-independent "static" disorder, reflecting the inhomogeneous structure of the NPs.[10] As we show below, however, this interpretation is problematic. For example, the Pt−Pt bond strengths $k \propto \Theta_E^2$ based on Einstein models (EMs) of the MSRD with Einstein temperatures Θ_E are anomalous. Indeed, fits for 0.9 nm NPs gave an anomalously large Θ_E = 300 K, equivalent to a mean vibrational frequency ν_E = 6.3 THz. This mean frequency is larger than that observed for the strongest known Pt−Pt bonds and is hence unphysical. Similarly, the Grüneisen parameters[11] γ derived from the variation of the ν_E with cluster size are anomalous, being >50% larger than in bulk.

We show here that this seemingly anomalous behavior of the MSRD can be accounted for by a reinterpretation of the dynamic disorder. The MSRD σ_P^2 for a single Pt_i−Pt_j (i,j = 1...N) bond trajectory $r_P(t) = |\vec{r}_i(t) - \vec{r}_j(t)|$ is defined as the time average

$$\sigma_P^2(T) = \frac{1}{\tau}\int_0^\tau [r_P(t) - \bar{r}_P]^2\, dt \qquad (1)$$

where $P = \{i,j\}$ denotes a bond pair and $\bar{r}_P$ is the mean bond distance computed as a time average over the same long-time time τ (10 ps in our simulations). To obtain the total MSRD $\sigma^2_{Tot}(T)$, we average over all initial conditions and over pair trajectories chosen to minimize tail effects (see the Supporting Information)

Received: June 7, 2017
Accepted: July 1, 2017
Published: July 2, 2017

DOI: 10.1021/acs.jpclett.7b01446
J. Phys. Chem. Lett. 2017, 8, 3284−3288

$$\sigma^2_{\mathrm{Tot}}(T) = \left\langle \frac{1}{N_P} \sum_P \sigma^2_P(T) \right\rangle \quad (2)$$

where the brackets indicate the average over initial conditions. We show that in addition to low-frequency dynamic fluctuations, the MSRD also contains a temperature-dependent quasi-equilibrium component, which we dub anomalous structural disorder (ASD). To compute the ASD and analyze its origin, we perform a spectral analysis of the temperature and size dependence of the different components of disorder in supported Pt NPs. We partition the MSRD into three components according to their dynamic time scales: vibrational disorder (σ^2_{Vib}) associated with fast nuclear motion with frequencies higher than 1 THz, dynamic structural disorder (σ^2_{DSD}) arising from slower dynamics in the 0 to 1 THz range, and ASD (σ^2_{ASD}) associated with mean quasi-static Pt−Pt disorder over the duration of the simulation. The partitioning is done by convolving a trajectory $r(t)$

$$r_{\mathrm{L}}(t) = \int_{-\infty}^{+\infty} r(\tau) F(t-\tau)\, \mathrm{d}\tau \quad (3)$$

with a low-pass filtering function $F(t)$ defined as

$$F(t) = \begin{cases} \frac{\pi}{2}\nu_{\mathrm{L}} \cos(\pi\nu_{\mathrm{L}} t) & |t| < 1/2\nu_{\mathrm{L}} \\ 0 & |t| > 1/2\nu_{\mathrm{L}} \end{cases} \quad (4)$$

Here ν_{L} is the cutoff frequency (set to 1 THz) and $r_{\mathrm{L}}(t)$ is the low-frequency component of the trajectory. From $r_{\mathrm{L}}(t)$ we define the high-frequency component as $r_{\mathrm{H}}(t) = r(t) - r_{\mathrm{L}}(t)$. The partitioned σ^2_{Vib} and σ^2_{DSD} are obtained similarly to σ^2_{P} in eq 1. The ASD component is defined as

$$\sigma^2_{\mathrm{ASD}}(T) = \langle (\bar{r}_{\mathrm{L}} - \langle \bar{r}_{\mathrm{L}} \rangle)^2 \rangle \quad (5)$$

where the brackets indicate an average over all selected trajectories and initial conditions and where the mean trajectory distance $\bar{r}_{\mathrm{L}}$ is

$$\bar{r}_{\mathrm{L}} = \frac{1}{\tau} \int_0^{\tau} r_{\mathrm{L}}(t)\, \mathrm{d}t \quad (6)$$

A simpler version of this partitioning that did not separate the ASD from DSD was previously used[9,12] to investigate dynamic effects on Pt and PtSn NPs.

Physically the effective pair potentials in NPs depend strongly on the NP−support interaction and other environmental factors that make them indirectly temperature-dependent, similar to the temperature dependence of the mean geometrical structure in the quasi-harmonic approximation. We show that the apparent anomalous MSRD behavior arises from neglecting the temperature dependence of the ASD and disappears when the ASD is taken into account. Thus the ASD is critically important in attaining an all-encompassing explanation for understanding NP properties including NTE, MSRD, and γ. Consequently, we propose that, although widely used the NP community, the concept of temperature-independent static disorder should be revised because it yields incorrect behavior for small supported NPs.

To study the behavior of the NPs under realistic conditions, we carried out DFT/MD simulations of γ-Al_2O_3-supported Pt_{10} and Pt_{20} clusters for temperatures ranging from 165 to 573 K. Given that acquiring adequate statistics, especially at lower temperatures, requires careful sampling,[13] the results for each temperature are obtained by averaging over six independent trajectories starting from different initial conditions. (See the Computational Methods section.) Figure 1 shows the total

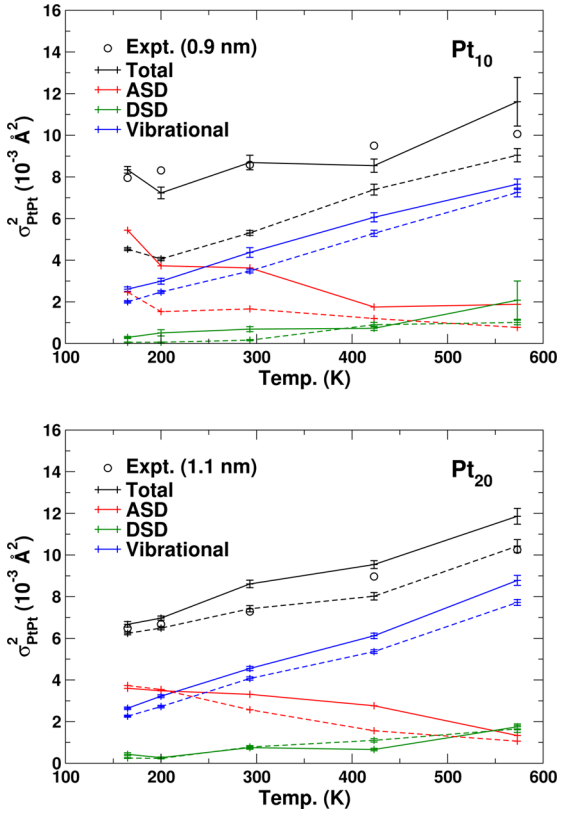

Figure 1. Decomposition of the Pt−Pt MSRD for supported (full) and unsupported (dashed) Pt_{10} (top) and Pt_{20} (bottom) clusters. The vibrational component corresponds to disorder with frequencies above 1 THz, the DSD to that between 0 and 1 THz, and the quasi-equilibrium ASD component to dynamics that are longer than the length of these simulations. The experimental values were taken from ref 7. The error bars correspond to estimated errors in the mean.

MSRD averaged over all internal bonds for both supported and unsupported Pt_{10} and Pt_{20}. We find that the diameter cutoffs for finding 95% of the atoms are 0.82 and 1.04 nm for Pt_{10} and Pt_{20}, respectively. Thus these results are compared with those measured for the 0.9 and 1.1 nm NPs[7] and found to be in reasonable agreement, with an average error of ∼10%.

The conventional way to estimate mean bond strength in EXAFS experiments is to fit the EXAFS $\sigma^2(T)$ to an EM plus an additional temperature-independent "static-disorder" term σ^2_{S}[14−16]

$$\sigma^2(T) = \sigma^2_{\mathrm{S}} + \frac{\hbar^2}{2\mu k_{\mathrm{B}}} \frac{1}{\Theta_{\mathrm{E}}} \coth\left(\frac{\Theta_{\mathrm{E}}}{2T}\right) \quad (7)$$

Here μ is the reduced mass of a Pt−Pt pair, k_{B} is Boltzmann's constant, and $\Theta_{\mathrm{E}} = h\nu_{\mathrm{E}}/k_{\mathrm{B}}$ is the Einstein temperature. However, this approach becomes questionable when the system is inhomogeneous and σ^2_{S} has significant contributions from DSD.[17] This inhomogeneity is difficult to determine experimentally since EXAFS gives global average quantities. Our simulations show, however, that the NPs have distinct populations of surface and interior atoms and bonds (Supplementary Figures S1 and S2). One of our key findings is that the NPs undergo a smooth homogenizing transition with

DOI: 10.1021/acs.jpclett.7b01446
J. Phys. Chem. Lett. 2017, 8, 3284−3288

Table 1. Einstein Model Fit Parameters for the Total and Decomposed MSRDs of Supported and Unsupported Pt_{10} and Pt_{20}, and for Bulk Pt[a]

comp.	param.		Pt_{10}/γ-Al_2O_3	Pt_{20}/γ-Al_2O_3	Pt_{10}	Pt_{20}	Pt foil
σ^2_{Tot}	Θ_E	theo.	239 ± 76	197 ± 14	198 ± 18	221 ± 26	184 ± 4
		expt.	300 ± 22	223 ± 12			181 ± 2
	σ^2_S	theo.	5.8 ± 2.0	4.3 ± 0.6	1.7 ± 0.8	4.2 ± 0.8	0.0 ± 0.2
		expt.	6.9 ± 0.4	4.5 ± 0.4			0.2 ± 0.2
σ^2_{Vib}	Θ_E	theo.	196 ± 8	182 ± 7	193 ± 3	192 ± 8	
σ^2_{DSD}	Θ_E	theo.	81 ± 22	63 ± 18	96 ± 10	59 ± 5	

[a]Einstein temperatures (Θ_E) in K; static disorder (σ^2_S) in 10^{-3} Å^2. Errors correspond to the 95% confidence interval. The σ^2_S for σ^2_{Vib} and σ^2_{DSD} are statistically indistinguishable from 0. Experimental data refitted from ref 7.

temperature, resulting in a quasi-static $\sigma^2_S(T)$ that is temperature-dependent. Therefore, the conventional interpretation of fitted EM plus "static disorder" in terms of bond strengths is unreliable and must be modified. To demonstrate this for small NPs, the parameters for traditional EM fits are given in Table 1. The simulations reproduce the large σ^2_S observed in the experiment within error bars, and their fitted Θ_E have the correct decreasing trend with increasing size, although slightly lower than experiment. The bonds in unsupported Pt_{10} are weaker and become less disordered with increasing temperature than those on the support. In contrast, results for supported and unsupported Pt_{20} are similar. Our simulations also reproduce bulk Pt with smaller Θ_E and no static disorder.

Assuming the conventional EM interpretation for the sake of argument, the fitted Θ_E = 300 K for Pt_{10} would imply an effective vibrational frequency of 6.3 THz, which is much higher than the ν_E = 3.8 THz observed for the bulk. Such an increase is consistent with well known many-body bonding effects[18,19] that result in bond strengthening with reduced coordination number.[20−22] That is, the smaller the system, the lower the mean coordination of the bonds and higher ν_E (Supplementary Figures S3 and S4).[12,13] However, the observed ν_E are too high to be physically plausible: A value of 6.3 THz in Pt_{10} is comparable to that in the strongly bound isolated Pt_2 dimer,[23] which is 5.8 THz in a supercooled jet[24] and 6.5 THz in a noble-gas matrix.[25]

Figure 1 also shows the components of the MSRD as a function of temperature, while the parameters for their EM fits are presented in Table 1. σ^2_{Vib} shows normal behavior for both supported and unsupported systems, with a Θ_E 45 K lower for Pt_{10} than that for the total MSRD. In fact, σ^2_{Vib} is quite similar to that in the bulk, with a Θ_E of 196 K versus the bulk value of 184 K. The small difference arises from the shorter and stronger cluster bonds. The σ^2_{DSD} also shows normal linear behavior with increasing temperature, although with a significantly smaller slope than σ^2_{Vib}. Given that the DSD originates from low-frequency dynamics associated with the motion of the CM (see the Supporting Information), we use the total mass of the cluster in the EM fits instead of the Pt−Pt reduced mass, resulting in a Θ_E of about 60−80 K.

Of the three components of the MSRD, the ASD component is the only anomalous one, decreasing with increasing temperature and explaining the enhanced Θ_E. For Pt_{10}, σ^2_{ASD} accounts for 70% of the total disorder at low temperature, decreasing linearly to 15% at high temperature. The σ^2_{ASD} in unsupported Pt_{10} is about half, showing that the support has a very large effect on the MSRD of small NPs. In contrast, the supported and unsupported Pt_{20} clusters show both a much smaller variation with temperature and similar σ^2_{ASD}. These results highlight two important observations: First, σ^2_{ASD} is the only component that has significant size and support dependence. Second, the temperature variation of σ^2_{ASD} for Pt_{20} is already quite small, indicating that standard EXAFS analysis methods are likely valid for NPs with 40 atoms or more. To probe the origin of the temperature dependence of σ^2_{ASD}, Figure 2 shows the $\bar{r}_L$ distribution as a function of temperature. The σ^2_{ASD} decrease appears as a narrowing of the distribution caused by two main effects: (i) the longer/weaker bonds are preferentially removed from the screening window as they become active and (ii) the shorter bonds become longer due to thermal expansion. The NTE of the NPs is visible as a left shift of the centroid of the distributions (Supplementary Figure S4, bottom).

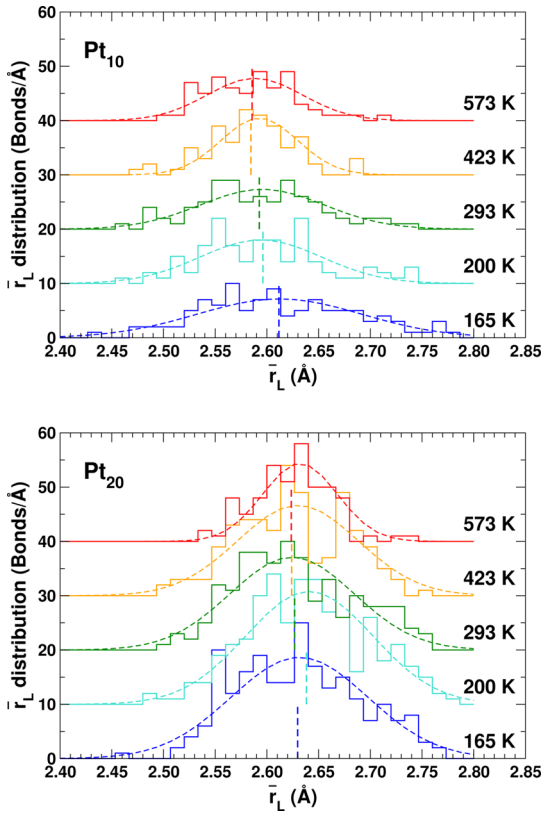

Figure 2. Comparison of the equilibrium pair distribution functions as a function of temperature for Pt_{10} (top) and Pt_{20} (bottom). Also included are Gaussian fits and vertical lines (dashed) indicating the spread and centroid of the distributions, respectively.

Finally, we discuss the anomalous Grüneisen parameter γ

DOI: 10.1021/acs.jpclett.7b01446
J. Phys. Chem. Lett. 2017, 8, 3284−3288

$$\gamma = -\frac{d \ln \nu_E}{d \ln V} = -\frac{1}{3}\frac{d \ln \nu_E}{d \ln R_{PtPt}} \quad (8)$$

which characterizes bond anharmonicity. Estimates of γ based on ν_E values from standard EM fits of the total MSRDs give γ values of 5 ± 2 and 4 ± 2 from experiment and theory, respectively. These estimates are counterintuitively larger than the γ = 2.7 measured for the solid.[26] On the basis of simple effective anharmonic potential models,[27] γ can be approximated as $\gamma = k_3R/k_2$, where k_2 and k_3 are, respectively, the harmonic and anharmonic force constants of the effective potential. Thus given that in the NPs R is smaller and k_2 is larger, if we assume that the anharmonicity remains about the same, then we expect $\gamma_{NP} < \gamma_{Bulk}$. The anomalous values can be traced to the assumption of temperature-independent static disorder in the EM fits; however, normal behavior is recovered when actual vibrational ν_E values are used. Figure 3 shows the variation of ν_E

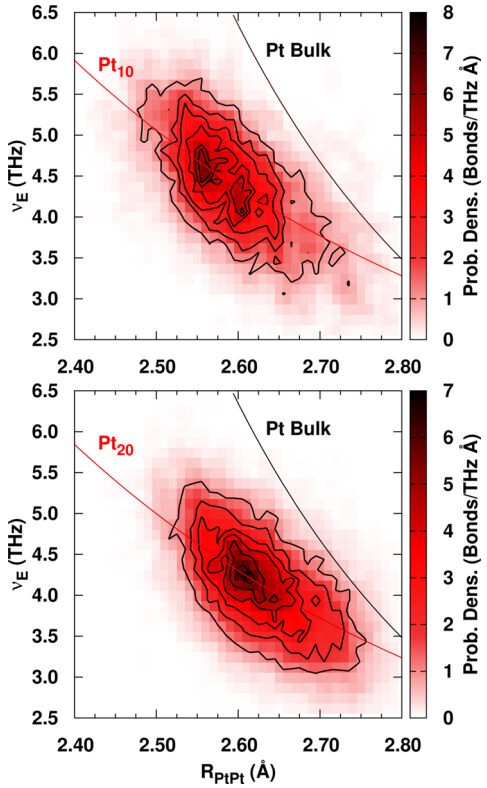

Figure 3. Probability distribution of the mean vibrational frequency ν_E of a Pt−Pt bond as a function of its mean bond length R_{PtPt}. The black line for bulk Pt was obtained by assuming a constant γ = 2.7 and a ν_E = 3.8 THz at 2.77 Å. The red lines correspond to fits of the Pt_{10} and Pt_{20} data also assuming a constant γ.

as a function of R_{PtPt} for Pt_{10} and Pt_{20} compared with the variation for bulk Pt obtained by assuming a constant γ = 2.7 and ν_E = 3.8 THz at 2.77 Å. The NP ν_E values were obtained as the mean frequencies of 1 ps wavelets generated from the $r_H(t)$ trajectories. Although the NPs exhibit a broad distribution of frequencies due to the bond length range, they show the expected inverse relationship between bond length and frequency. The distributions peak at the Pt_{10} and Pt_{20} mean R_{PtPt} distances of 2.60 and 2.63 Å, with mean frequencies of 4.4 and 4.1 THz, respectively, in reasonable agreement with the values of 4.1 ± 0.2 and 3.8 ± 0.2 THz obtained from EM fits of σ^2_{Vib}. The red lines in Figure 3 correspond to fits of ν_E versus R_{PtPt} assuming constant γ, which we find to be 1.3 ± 0.5 for both Pt_{10} and Pt_{20}, thus lower than the bulk value, as expected from anharmonicity considerations.

In summary, we carried out DFT/MD simulations of supported Pt NPs as a function of size and temperature and analyzed their dynamic behavior by partitioning the MSRD of the Pt−Pt bonds into vibrational, DSD, and ASD components. We show that the vibrational contribution arises from local Pt−Pt vibrations and is primarily controlled by the number of NN around the bonds. The DSD component, conversely, arises from the coupling between the global CM dynamics with the local Pt−Pt bond fluctuations. The ASD is due to the fraction of bonds that remain "frozen" for >10 ps at a given temperature and decreases linearly with increasing temperature. Our simulations reveal large inhomogeneity in the NPs, showing distinct surface and interior atom populations, thus challenging the conventional interpretation of bond strengths from EM fits with static disorder that leads to anomalous values. Instead we found that the heretofore so-called static component is not constant but decreases with temperature. This decrease in the ASD component is caused by two effects: (i) the activation of the longer, weaker Pt−Pt bonds and (ii) the stretching of the shorter bonds. This results in a narrowing of the equilibrium bond-distance distribution with increasing temperature, and, given that it is dominated by the former, the system experiences an effective NTE. Physically this behavior is analogous to a smooth phase transition to a more homogeneous structure with increasing temperature. In contrast, the DSD and vibrational components display normal thermal behavior, with the vibrational component being similar to that in bulk Pt and the DSD contributing about 10−20% of the total MSRD. Thus to obtain bond-strength-associated Grüneisen parameters from EXAFS, one has to subtract both the DSD and ASD components of the disorder. Finally, given that these anomalous properties likely arise from the synergistic effects of limited dimensionality of these systems,[9] intraparticle heterogeneity,[28] and the effects of oxide support, our results suggest the existence of other particle−support systems with similar anomalous properties.

COMPUTATIONAL METHODS

The computational approach here is similar to that used previously:[13] All ab initio DFT/MD runs were done using VASP[29] using the Nosé−Hoover thermostat[30,31] and the PBE functional.[32] The simulations were nonrelativistic and used spin-unpolarized densities at the Γ point, ultrasoft pseudopotentials, and a plane-wave cutoff of 297 eV. (See the Supporting Information for more detailed information.) The initial structures for each temperature were generated by creating random clusters with appropriate bond distances (2.5 to 2.9 Å), which were then placed onto the "d" layer of the dehydroxylated [110] surface of γ-Al_2O_3 and fully optimized before starting the MD runs. The γ-Al_2O_3 surface is represented by four layers (two fully relaxed and two frozen) in a supercell of 19.4 Å × 13.7 Å, with an effective vacuum separation of 16 Å. Each run was 20 ps long, with the first 10 ps used for thermalization and discarded from the analysis. The equations of motion were integrated with the velocity-Verlet method with a 3 fs time step, which captures the fastest fluctuations at the highest temperatures studied. In addition, we also carried out DFT/MD simulations for unsupported Pt_{10}, Pt_{20}, and bulk Pt. These runs used the same computational details as those on γ-Al_2O_3, except that their simulation cells were different: For

DOI: 10.1021/acs.jpclett.7b01446
J. Phys. Chem. Lett. 2017, 8, 3284−3288

unsupported Pt_{10} and Pt_{20} we used a cubic cell with side 15 Å, while for bulk Pt we used a cubic simulation cell with side 11.898 Å and 108 atoms (a 3 × 3 × 3 replica of the conventional Pt cell).

■ ASSOCIATED CONTENT

Supporting Information

The Supporting Information is available free of charge on the ACS Publications website at DOI: 10.1021/acs.jpclett.7b01446.

Description of tail removal. Discussion of the relation between CM dynamics and disorder. Origin of sub-terahertz dynamics. Discussion of XC computational settings. Figures describing the internal structure of the NPs. (PDF)

■ AUTHOR INFORMATION

Corresponding Author

*E-mail: fdv@uw.edu.

ORCID

Fernando D. Vila: 0000-0002-6508-4896

Anatoly I. Frenkel: 0000-0002-5451-1207

Notes

The authors declare no competing financial interest.

■ ACKNOWLEDGMENTS

This work was supported by U.S. Department of Energy, Office of Science CSGBD Grant No. DE-FG02-03ER15476, with computational support from NERSC, a DOE Office of Science User Facility, under Contract No. DE-AC02-05CH11231. A.I.F. acknowledges support from Program Development funding at Brookhaven National Laboratory under U.S. Department of Energy Contract No. DE-SC0012704. We thank J. J. Kas for many helpful discussions.

■ REFERENCES

(1) Antos, G.; Aitani, A. *Catalytic Naphtha Reforming*; Chemical Industries Series; Marcel Dekker, Inc., 2004.

(2) Schlögl, R.; Abd Hamid, S. B. Nanocatalysis: Mature Science Revisited or Something Really New? *Angew. Chem., Int. Ed.* **2004**, *43*, 1628−1637.

(3) Duan, Z.; Li, Y.; Timoshenko, J.; Chill, S. T.; Anderson, R. M.; Yancey, D. F.; Frenkel, A. I.; Crooks, R. M.; Henkelman, G. A Combined Theoretical and Experimental EXAFS Study of the Structure and Dynamics of Au_{147} Nanoparticles. *Catal. Sci. Technol.* **2016**, *6*, 6879−6885.

(4) Chill, S. T.; Anderson, R. M.; Yancey, D. F.; Frenkel, A. I.; Crooks, R. M.; Henkelman, G. Probing the Limits of Conventional Extended X-ray Absorption Fine Structure Analysis Using Thiolated Gold Nanoparticles. *ACS Nano* **2015**, *9*, 4036−4042.

(5) Yancey, D. F.; Chill, S. T.; Zhang, L.; Frenkel, A. I.; Henkelman, G.; Crooks, R. M. A Theoretical and Experimental Examination of Systematic Ligand-Induced Disorder in Au Dendrimer-Encapsulated Nanoparticles. *Chem. Sci.* **2013**, *4*, 2912−2921.

(6) Kang, J. H.; Menard, L. D.; Nuzzo, R. G.; Frenkel, A. I. Unusual Non-Bulk Properties in Nanoscale Materials: Thermal Metal-Metal Bond Contraction of γ-Alumina-Supported Pt Catalysts. *J. Am. Chem. Soc.* **2006**, *128*, 12068−12069.

(7) Sanchez, S. I.; Menard, L. D.; Bram, A.; Kang, J. H.; Small, M. W.; Nuzzo, R. G.; Frenkel, A. I. The Emergence of Nonbulk Properties in Supported Metal Clusters: Negative Thermal Expansion and Atomic Disorder in Pt Nanoclusters Supported on γ-Al_2O_3. *J. Am. Chem. Soc.* **2009**, *131*, 7040−7054.

(8) Vila, F. D.; Rehr, J. J.; Kas, J. J.; Nuzzo, R. G.; Frenkel, A. I. Dynamic Structure in Supported Pt Nanoclusters: Real-time Density Functional Theory and X-Ray Spectroscopy Simulations. *Phys. Rev. B: Condens. Matter Mater. Phys.* **2008**, *78*, 121404.

(9) Rehr, J. J.; Vila, F. D. Dynamic Structural Disorder in Supported Nanoscale Catalysts. *J. Chem. Phys.* **2014**, *140*, 134701.

(10) Gilbert, B.; Huang, F.; Zhang, H.; Waychunas, G. A.; Banfield, J. F. Nanoparticles: Strained and Stiff. *Science* **2004**, *305*, 651−654.

(11) Chernyshev, A. The Mie-Grüneisen Equation of State for Metal Nanoparticles. *Eur. Phys. J. B* **2011**, *79*, 321−325.

(12) Vila, F. D.; Rehr, J. J.; Kelly, S. D.; Bare, S. R. Operando Effects on the Structure and Dynamics of Pt_nSn_m/γ-Al_2O_3 from Ab Initio Molecular Dynamics and X-ray Absorption Spectra. *J. Phys. Chem. C* **2013**, *117*, 12446−12457.

(13) Vila, F. D.; Hayashi, S. T.; Moore, J. M.; Rehr, J. J. Molecular Dynamics Simulations of Supported Pt Nanoparticles with a Hybrid Sutton-Chen Potential. *J. Phys. Chem. C* **2016**, *120*, 14883−14891.

(14) Sevillano, E.; Meuth, H.; Rehr, J. Extended X-Ray Absorption Fine Structure Debye-Waller Factors. I. Monatomic Crystals. *Phys. Rev. B: Condens. Matter Mater. Phys.* **1979**, *20*, 4908−4911.

(15) Frenkel, A.; Rehr, J. Thermal Expansion and X-Ray-Absorption Fine-Structure Cumulants. *Phys. Rev. B: Condens. Matter Mater. Phys.* **1993**, *48*, 585−588.

(16) Van Hung, N.; Rehr, J. Anharmonic Correlated Einstein-Model Debye-Waller Factors. *Phys. Rev. B: Condens. Matter Mater. Phys.* **1997**, *56*, 43−46.

(17) Price, S. W. T.; Zonias, N.; Skylaris, C.-K.; Hyde, T. I.; Ravel, B.; Russell, A. E. Fitting EXAFS Data Using Molecular Dynamics Outputs and a Histogram Approach. *Phys. Rev. B: Condens. Matter Mater. Phys.* **2012**, *85*, 075439.

(18) Ferrando, R.; Jellinek, J.; Johnston, R. L. Nanoalloys: From Theory to Applications of Alloy Clusters and Nanoparticles. *Chem. Rev.* **2008**, *108*, 845−910.

(19) Nørskov, J.; Jacobsen, K.; Stoltze, P.; Hansen, L. Many-Atom Interactions in Metals. *Surf. Sci.* **1993**, *283*, 277−282.

(20) Goldschmidt, V. Krystallbau und Chemische Zusammensetzung. *Ber. Dtsch. Chem. Ges. B* **1927**, *60*, 1263−1296.

(21) Pauling, L. Atomic Radii and Interatomic Distances in Metals. *J. Am. Chem. Soc.* **1947**, *69*, 542−553.

(22) Feibelman, P. J. Relaxation of hcp(0001) Surfaces: A Chemical View. *Phys. Rev. B: Condens. Matter Mater. Phys.* **1996**, *53*, 13740−13746.

(23) Yang, S. H.; Drabold, D. A.; Adams, J. B.; Ordejón, P.; Glassford, K. Density Functional Studies of Small Platinum Clusters. *J. Phys.: Condens. Matter* **1997**, *9*, L39−L45.

(24) Taylor, S.; Lemire, G. W.; Hamrick, Y. M.; Fu, Z.; Morse, M. D. Resonant Two-Photon Ionization Spectroscopy of Jet-Cooled Pt_2. *J. Chem. Phys.* **1988**, *89*, 5517−5523.

(25) Jansson, K.; Scullman, R. Optical Absorption Spectra of PtO and Pt_2 in Rare-Gas Matrices. *J. Mol. Spectrosc.* **1976**, *61*, 299−312.

(26) Wang, Z.; Lazor, P.; Saxena, S. A Simple Model for Assessing the High Pressure Melting of Metals: Nickel, Aluminum and Platinum. *Phys. B* **2001**, *293*, 408−416.

(27) Vila, F. D.; Rehr, J. J.; Rossner, H. H.; Krappe, H. J. Theoretical X-Ray Absorption Debye-Waller Factors. *Phys. Rev. B: Condens. Matter Mater. Phys.* **2007**, *76*, 014301.

(28) Elsen, A.; Jung, U.; Vila, F. D.; Li, Y.; Safonova, O. V.; Thomas, R.; Tromp, M.; Rehr, J. J.; Nuzzo, R. G.; Frenkel, A. I. Intracluster Atomic and Electronic Structural Heterogeneities in Supported Nanoscale Metal Catalysts. *J. Phys. Chem. C* **2015**, *119*, 25615−25627.

(29) Kresse, G.; Furthmüller, J. Efficient Iterative Schemes for Ab Initio Total-Energy Calculations Using a Plane-Wave Basis Set. *Phys. Rev. B: Condens. Matter Mater. Phys.* **1996**, *54*, 11169−11186.

(30) Nosé, S. A Unified Formulation of the Constant Temperature Molecular Dynamics Methods. *J. Chem. Phys.* **1984**, *81*, 511−519.

(31) Hoover, W. G. Canonical Dynamics: Equilibrium Phase-Space Distributions. *Phys. Rev. A: At., Mol., Opt. Phys.* **1985**, *31*, 1695−1697.

(32) Perdew, J. P.; Burke, K.; Ernzerhof, M. Generalized Gradient Approximation Made Simple. *Phys. Rev. Lett.* **1996**, *77*, 3865−3868.